

Robust integration of fast flavor conversions in classical neutrino transport

Zewei Xiong^{1,*}, Meng-Ru Wu^{2,3,4,†}, Manu George^{2,‡} and Chun-Yu Lin^{5,§}

¹*GSI Helmholtzzentrum für Schwerionenforschung, Planckstraße 1, 64291 Darmstadt, Germany*

²*Institute of Physics, Academia Sinica, Taipei 11529, Taiwan*

³*Institute of Astronomy and Astrophysics, Academia Sinica, Taipei 10617, Taiwan*

⁴*Physics Division, National Center for Theoretical Sciences, Taipei 10617, Taiwan*

⁵*National Center for High-performance Computing, Hsinchu 30076, Taiwan*

(Dated: March 27, 2024)

The quantum kinetic evolution of neutrinos in dense environments, such as the core-collapse supernovae or the neutron star mergers, can result in fast flavor conversion (FFC), presenting a significant challenge to achieving robust astrophysical modeling of these systems. Recent works that directly simulate the quantum kinetic transport of neutrinos in localized domains have suggested that the asymptotic outcome of FFCs can be modeled by simple analytical prescriptions. In this *Letter*, we incorporate the analytical prescriptions into global simulations that solve the classical neutrino transport equation including collisions and advection under spherical symmetry. We demonstrate excellent agreement between results obtained using this approach and those directly from the corresponding global quantum kinetic simulations. In particular, this effective method can also precisely capture the collisional feedback effect for cases where the FFC happens inside the neutrinosphere. Our work highlights that a robust integration of FFCs in classical neutrino transport used in astrophysical simulation can be feasible.

Introduction.— The robustness of astrophysical simulations for explosive events such as core-collapse supernovae (CCSNe) and neutron star mergers (NSMs) relies on the accurate numerical modeling of the non-equilibrium classical neutrino transport from the neutrino-trapped to free-streaming regime [1–7]. However, recent studies have revealed that the quantum mechanical nature of neutrinos, as manifested in their flavor oscillations, can lead to various collective modes of flavor conversions in regions where neutrinos decouple from matter [8–10]. These collective phenomena, originated from the nonlinear self-interaction of neutrino forward scattering, may significantly affect the theoretical modeling of CCSNe and NSMs, thus emphasizing the need for quantum kinetic transport of neutrinos [11–16].

In particular, the so-called fast flavor instability (FFI) [17–20] can exist at locations where the angular distribution of the neutrino electron lepton number (ELN) density contains a crossing, i.e., the ELN angular distribution function changes sign [21, 22], and is commonly found in the interior of CCSNe and NSM remnants [23–35]. The presence of FFI can lead to the emergence of fast flavor conversion (FFC) and alter the neutrino flavor content within a timescale of subnanosecond and a length scale of subcentimeter, much shorter than the typical hydrodynamical or interaction time and length scales governed by classical processes.

The large separation of scales implies an exceedingly high computational cost for a direct implementation of neutrino quantum kinetic transport in CCSN and NSM simulations. Intensive studies aimed to obtain solutions to this problem have been explored. A large number of recent works have numerically solved the neutrino quantum kinetic equation (ν QKE) in localized simulation domains to understand the outcome of FFCs [36–52]. Attempts

to model the FFC outcome based on these simulations using analytical formulas [37, 47, 49, 53] or through the use of machine learning [54, 55] have proven that accurate FFC outcomes relevant to the modeling of neutrino transport can be obtained. Global transport simulations solving ν QKE with different simplifications, e.g., using artificially quenched neutrino self-interaction or adopting spatial resolutions lower than the FFC length scales, have been performed [56–63] and provided improved understanding of the emergence and evolution of FFCs in static background. On the other hand, preliminary efforts to include the FFC outcome in parametric fashions in hydrodynamical simulations equipped with classical neutrino transport solvers were conducted in [64–68]. Moreover, theoretical frameworks of subgrid methods have been recently proposed in [50, 69, 70].

Despite all these tremendous efforts, an important question that remains to be answered is whether or not the FFC outcome learned from local ν QKE simulations can be effectively included in classical transport used in astrophysical simulations. In this *Letter*, we tackle this question by incorporating analytical prescriptions into global simulations that solve the classical neutrino transport equation under spherical symmetry. For the first time, we show *robust* agreement between results from this approach and those directly solving the ν QKE in our earlier work [61], which reveals the viability of effective integration of FFC in astrophysical simulations.

Model.— We use COSE ν [71] to numerically solve both the ν QKE and the corresponding classical transport equation under the same spherically symmetric CCSN background profiles based on a $25M_{\odot}$ progenitor as used in [61]. The ν QKE simulations are performed in a radial range from $r = 20$ km to 80 km, spanning both the neutrino-trapped and free-streaming regimes. The

setup and the analyses of the FFC results have been described in detail in [61] for several models with different ELN angular distributions. Here we focus on Models II, III, and IV of [61] obtained under the two-flavor scheme. We use the attenuation function $a_{\nu\nu}(r)$ to quench the strength of the neutrino-neutrino forwarding scattering Hamiltonian, $\mathbf{H}_{\nu\nu}(v_r) = \sqrt{2}G_F \int dE' dv'_r (1 - v_r v'_r) [\varrho(E', v'_r) - \bar{\varrho}^*(E', v'_r)]$ with G_F the Fermi constant, E and v_r the energy and the radial velocity of neutrinos, and ϱ and $\bar{\varrho}$ the density matrices of neutrino and antineutrinos. Natural units with $\hbar = c = 1$ are adopted throughout this paper. Note that the diagonal elements of ϱ and $\bar{\varrho}$ are related to the neutrino and antineutrino number densities by $n_{\nu_i}(r, t) = \int dE dv_r \varrho_{ii}$ and $n_{\bar{\nu}_i}(r, t) = \int dE dv_r \bar{\varrho}_{ii}$ for $i = e, x$ with x denoting the heavy-lepton flavor. The attenuation function takes the form $a_{\nu\nu}(r) = a/[1 + e^{(30-r[\text{km}])/2.5}]$, such that $a_{\nu\nu}(r) \approx a$ at $r > 35$ km and $a_{\nu\nu}(r) > 0.1a$ at $r > 25$ km for the radial range where FFC occurs. In Models II and III, $n_{\nu_e} \gtrsim n_{\bar{\nu}_e}$ at all radii before FFCs, while $n_{\nu_e} \lesssim n_{\bar{\nu}_e}$ in Model IV, representing the ν_e and $\bar{\nu}_e$ dominating cases, respectively. Moreover, the FFIs exist inside the neutrinospheres in Models III and IV, which leads to an intriguing collisional feedback effect that continuously alters the evolution of neutrino distributions after the prompt FFC [61].

For the classical transport simulations that effectively take into account the outcome of FFC, we assume that when the FFI exists at any radius, i.e., when there exists an ELN angular crossing, the FFC quickly relaxes the neutrino flavor content to a local quasistationary state within a timescale much shorter than the collisional and the advection timescales. In the quasistationary state, the coarse-grained ELN angular distribution does not contain any crossings, and can be approximated by certain analytical prescriptions, where flavor equilibration takes place in a part of the angular domain [47, 49]. Based on this assumption, we then take the following practical procedures to effectively incorporate the FFC in the classical transport.

First, the coarse-grain nature allows us to take a larger radial grid size not limited by the size of $\mathbf{H}_{\nu\nu}$. Thus, in all our effective models, we use 2,500 radial grids in the simulation domain with a time step size $\Delta t = 32$ ns. Second, we only evolve the diagonal elements ϱ_{ii} and $\bar{\varrho}_{ii}$ by setting the coherent propagation Hamiltonian term, as well as the off-diagonal entries in the collision term to zero. Third, at each time step, we check whether there exist angular crossings in the ELN function $G(v_r) = \langle \varrho_{ee} \rangle_E - \langle \bar{\varrho}_{ee} \rangle_E - \langle \varrho_{xx} \rangle_E + \langle \bar{\varrho}_{xx} \rangle_E$, where $\langle \cdot \rangle_E$ denotes the energy-integrated quantities at all radial grids. If an ELN crossing is found at a given radius, we then assume that immediate flavor redistribution takes place due to FFC, and apply the power-1/2 prescription scheme derived in [49] to calculate the redistributed diagonal elements in ϱ and $\bar{\varrho}$. Specifically, under

the two-flavor scenario, the energy-independent survival probability for (anti-)neutrinos is given by

$$P(v_r, w) = \begin{cases} \frac{1}{2} & \text{for } v_<, \\ 1 - \frac{1}{2}h(|v_r - v_c|/w) & \text{for } v_>, \end{cases} \quad (1)$$

where the function $h(x) = (x^2 + 1)^{-1/2}$ and v_c is the crossing velocity at which $G(v_c) = 0$. In the above equation, $v_<$ ($v_>$) is defined as the v_r range over which the absolute value of the positive or negative ELN, $|I_+|$ or $|I_-|$, is smaller (larger). The quantities I_\pm are defined as $\int dv_r G(v_r) \Theta[\pm G(v_r)]$ with Θ denoting the Heaviside function. The parameter w can be calculated so that the conservation of ELN holds, i.e., $\int dv_r [2P(v_r, w) - 1]G(v_r) = I_+ + I_-$. Finally, with Eq. (1), the neutrino flavor content $\varrho_{ii}^{(f)}$ after the FFC are replaced by

$$\begin{aligned} \varrho_{ee} &\rightarrow \varrho_{ee}^{(f)} = \varrho_{ee}P + \varrho_{xx}(1 - P), \\ \varrho_{xx} &\rightarrow \varrho_{xx}^{(f)} = \varrho_{ee}(1 - P) + \varrho_{xx}P, \end{aligned} \quad (2)$$

for all energy grids at the radial grids where sizable ELN crossings with $(I_</I_>) > 10^{-3}$ are found, where $I_< = \min(|I_+|, |I_-|)$ and $I_> = \max(|I_+|, |I_-|)$. A similar redistribution applies to antineutrinos as well. We also note that Eq. (1) only applies to cases with at most a single angular crossing at any given radius, which is indeed true in all of our models examined in this work. Except for the procedures outlines above, all other settings in the classical transport simulations with FFCs are identical to those in the corresponding ν QKE simulations.

Results.— We run all the ν QKE simulations as well as the classical counterparts including the effective FFC implementation up to 320 μ s when the systems have settled into the asymptotic states. For ν QKE models, we take two different attenuation factors: $a = 4 \times 10^{-3}$ and $a = 10^{-3}$, which correspond to Models IIa4–IVa4 and Models II–IV listed in Table I of Ref. [61]. For the rest of the paper, we label the ν QKE models using larger (smaller) value of a as the “-H” (“-L”) models. For the effective classical models, they are labeled with “-C” after the model names, correspondingly. The ν QKE results shown in all figures are coarse-grain averaged over a size of 0.6 km.

Figure 1 compares the asymptotic radial profiles of the number density ratio between cases with FFCs and that with no flavor conversion, denoted as $n_\nu^{\text{FFC}}/n_\nu^{\text{NFC}}$ for all models. The FFC leads to more enhanced n_{ν_x} in Model IV, followed by Model III, and II in the ν QKE simulations. For ν_e and $\bar{\nu}_e$, since the FFC takes place at radii inside neutrinospheres in Model III and IV, the collisional feedback effect discussed in [61] can repopulate their number densities and work along with the subsequent FFC to largely alter the ELN distribution adiabatically after the prompt phase of FFC [see e.g., Fig. 2(d) and the discussion below]. As a result, the amount of reduction in n_{ν_e} and $n_{\bar{\nu}_e}$ are less so that their number

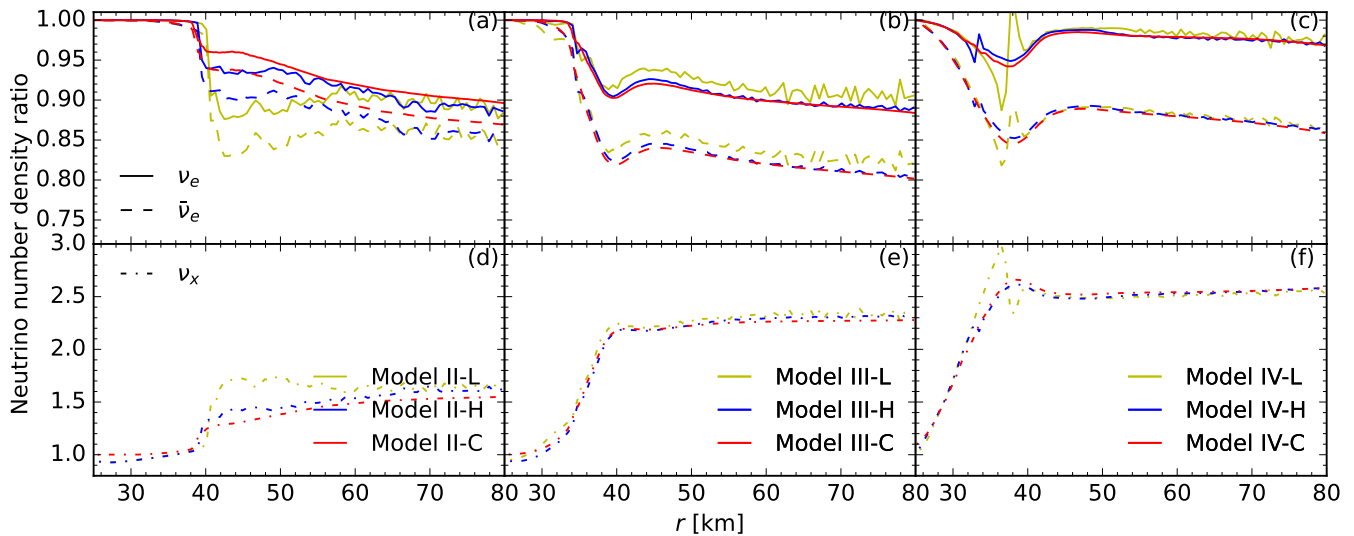


FIG. 1. Comparison of the radial profiles of neutrino number density ratios $n_\nu^{\text{FFC}}/n_\nu^{\text{NFC}}$ obtained in ν QKE simulations using different attenuation factors $a = 10^{-3}$ (yellow, labeled by “-L”) and $a = 4 \times 10^{-3}$ (blue, labeled by “-H”) with the corresponding classical transport simulation outcome taking into account the FFC effectively (red, labeled by “-C”) for ν_e , $\bar{\nu}_e$ [panel (a–c)] and ν_x [panel (d–f)] in Models II–IV, respectively.

density ratios in Models III and IV become comparable to those in Model II.

Comparing the effective classical results to the ν QKE ones, it clearly shows remarkably *quantitative* agreement in all three models. In particular, the differences in number density ratios between the -C and -H models are only up to $\lesssim 5\%$ in Model II, and are even smaller than 2% for most radii in Models III and IV, where the collisional feedback effects are important. For the -L ν QKE models, slightly larger differences exist around $r \simeq 45$ km in Model II and $r \simeq 37$ km in Model IV.

The differences in Model II are primarily associated with the flavor overconversion of the forward propagating neutrinos during the FFC, which occurs before the ELN distribution settles down to the quasistationary state that can be approximated by Eq. (1). With larger attenuation applied in the -L model, the lengthened FFC timescale prevents FFC from reaching the quasistationary state before advection takes effect. Consequently, larger amount of flavor overconversion is imprinted in the asymptotic state in Model II-L than in Model II-H. In Model IV, the negative ELN dominated by $\bar{\nu}_e$ ’s before FFCs changes to positive due to the collisional feedback. The strong attenuation of $\mathbf{H}_{\nu\nu}$ in -L model can cause the ELN to switch back to negative at $r \sim 30$ – 37 km, resulting in a sharp transition at $r \simeq 37$ km. However, in the -H model where less attenuation is adopted, the transition becomes less sharp and the location is shifted inwards to $r \simeq 33$ km. This indicates that the difference is related to the artificial attenuation and the modified ratios between the collisional rate and FFC rates. Overall, the better agreement in between the -C and -H models

than in between the -C and -L models suggests that in the -L models, the larger attenuation of $\mathbf{H}_{\nu\nu}$ may have quenched the FFC rate too much, particularly in Models II-L and IV-L.

To further illustrate the increasing agreement between the classical transport with effective FFC treatment and the ν QKE results with less attenuation, we show in Fig. 2 the comparison of the asymptotic neutrino angular distributions obtained at $r \simeq 44$ km in Model II and $r \simeq 41$ km in Model IV. In Model II-C, the reinforced flavor redistribution scheme leads to nearly equal amount of electron and heavy lepton flavors in both neutrino and antineutrino sectors in the velocity range $v_r \gtrsim v_c$. In both Models II-L and II-H, slight flavor overconversion is obtained. In Model IV, the collisional feedback leads to the gradual change of ELN distribution and v_c , so that flavor equilibration is reached at $v_r > v_c$ in the asymptotic state, in contrast to the range $v_r < v_c$ indicated by the ELN without FFCs [gray curve in Fig. 2(d)]. However, such an effect can be well reproduced in -C models as illustrated by panels (b) and (d). Once again, the results in the -H models clearly agree with those in the -C models better than the -L models.

Alternative effective schemes.— Besides the fiducial effective model used above, we have also performed two additional effective FFC implementation schemes in the classical transport simulations. The first set (labeled by “-C τ ”) is to involve an FFC timescale to relax the assumption of instantaneous flavor redistribution. The characteristic FFC timescale may be estimated by $\tau = G_F^{-1} |I_+ I_-|^{-1/2}$, which is proportional to the geometrical mean of the positive and negative ELNs [27, 50]. At

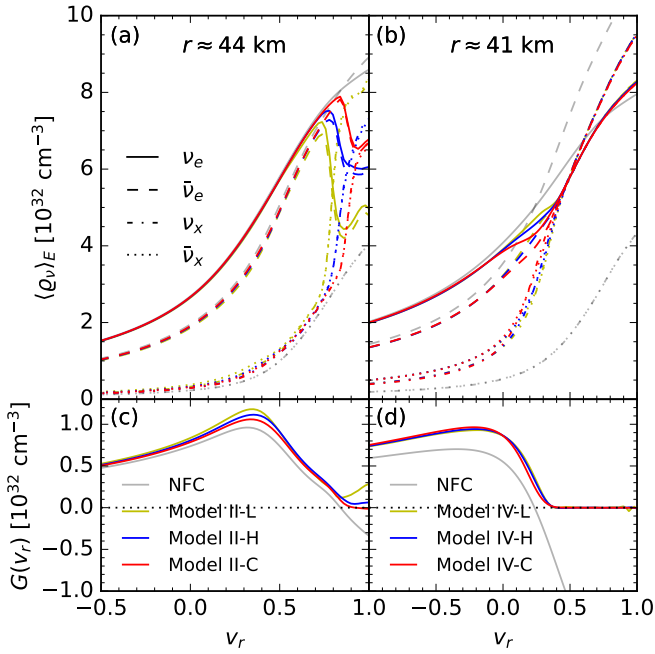


FIG. 2. The neutrino angular distributions for ν_e , ν_x , and their antineutrinos at $r \simeq 44$ km in Model II [panel (a)] and $r \simeq 41$ km in Model IV [panel (b)]. The corresponding ELN angular distributions are shown in panels (c) and (d) for Model II and IV. The yellow and blue curves are obtained in ν QKE simulations with attenuation factors $a = 10^{-3}$ (“-L” models) and $a = 4 \times 10^{-3}$ (“-H” models), respectively. The red curves are from the corresponding classical transport simulation outcome taking into account the FFC effectively (“-C” models). Note that we only plot v_r from -0.5 to 1 in (a) and (c) for better illustration.

each time step, we compute τ at where the ELN crossings are found and update the neutrino and antineutrino flavor content by $\varrho + (\varrho^{(f)} - \varrho) \min(\Delta t/\tau, 1)$ and $\bar{\varrho} + (\bar{\varrho}^{(f)} - \bar{\varrho}) \min(\Delta t/\tau, 1)$, respectively. When $\tau < \Delta t$, it reduces back to the instantaneous redistribution scheme. The results obtained with this method are nearly identical to those with instantaneous flavor redistribution in all models, see e.g., Fig. 3 for Model III. This comparison supports the validity of implementing instantaneous flavor redistribution in hydrodynamic simulations [64–68].

The second set of additional simulations is to use the “box” prescription [47] by setting $P(v_r) = 1 - I_{<}/(2I_{>})$ for $v_{>}$, labeled by “-Cb”. Interestingly, although the box prescription creates discontinuities in the local neutrino angular distribution functions [49] [see also Fig. 3(b)], the resulting neutrino densities do not differ substantially from those using the power-1/2 prescription, as shown in Fig. 3(a) for Model III. We have also examined that for other prescriptions that model the FFC outcome by continuous functions in [49], the results are nearly as good as those with the power-1/2 scheme.

Summary & discussions.— We have performed the first comparison of the global ν QKE simulations to the

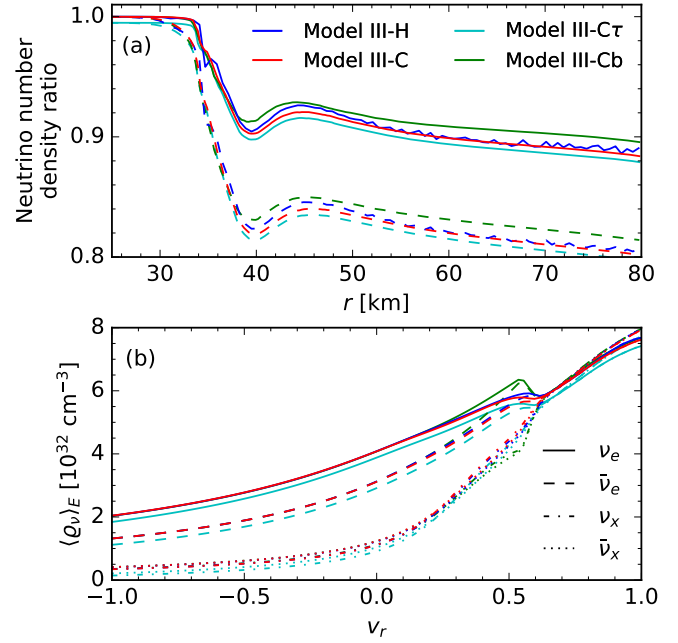


FIG. 3. The radial profiles of neutrino number density ratios $n_\nu^{\text{FFC}}/n_\nu^{\text{NFC}}$ [panel (a)] and the angular distributions at $r \simeq 41$ km [panel (b)] in Model III-H (blue), -C (red), -C τ (cyan), and -Cb (green). The -C τ model takes into account the FFC timescale. The -Cb model uses a different flavor redistribution scheme from the -C model. Note that because the curves for Model III-C τ completely overlap with those from the -C model, they are shifted by -0.005 in (a) and -0.2 in (b), respectively.

corresponding classical transport simulations that effectively take into account the outcome of the FFC. Our results showed that by implementing the analytical prescriptions proposed in [49] as the instantaneous FFC outcome into global simulation of classical neutrino transport that includes collisions and advection, remarkable agreements with the full ν QKE simulations can be obtained. The models that we examined in this work cover different cases with number densities dominated by ν_e or $\bar{\nu}_e$, and scenarios where the FFIs exist inside and outside neutrinospheres. In particular, the evolution of neutrino flavor content driven by the collisional feedback effect when the FFIs are located inside the neutrinospheres can also be robustly modeled by the effective classical transport method.

Moreover, we have found increasing agreement between the ν QKE results with less attenuation in the neutrino-neutrino forward scattering Hamiltonian with the results obtained by the effective classical transport method. Taking into account the characteristic FFC timescale or using different analytical prescription to describe the redistribution of neutrinos by FFC also gives rises to similar results in the effective classical transport models. Therefore, these suggest that the flavor redis-

tribution obtained on a coarse-grain level achieved in the FFC timescale in local FFC simulations with periodic boundary conditions can be used as a good proxy in global transport simulations that aim to include the impact of FFCs. The results presented here not only have validated the assumptions taken in preliminary works that tried to capture the potential impact of FFCs in hydrodynamic CCSN and NSM simulations, but also serve as a proof-of-principle study for the upcoming efforts to accurately identify the FFIs and integrate the FFC outcome utilizing machine learning and neural networks into the CCSN and NSM simulations equipped with classical two-moment neutrino transport schemes.

Despite the remarkable success presented above, it remains desired to explore whether flavor swap through the electron lepton zero surface [60, 72], or the adiabatic flavor transformation due to the temporal evolution of the environment [73] can be treated effectively as well. If a non-negligible amount of flavor overconversion due to FFC may exist for certain ELN distributions that cannot be described by analytical prescription schemes, it remains to be seen whether machine-learning based methods can accurately predict the related FFC outcome. All these are beyond the scope of this work but will be pursued in upcoming studies.

We thank Tobias Fischer and Noshad Khosravi Largani for providing the supernova profile. We are grateful for discussions with Sajad Abbar and Gabriel Martínez-Pinedo. ZX acknowledges support of the European Research Council (ERC) under the European Union’s Horizon 2020 research and innovation programme (ERC Advanced Grant KILONOVA No. 885281), the Deutsche Forschungsgemeinschaft (DFG, German Research Foundation) – Project-ID 279384907 – SFB 1245, and MA 4248/3-1. MRW and MG acknowledge supports from the National Science and Technology Council, Taiwan under Grant No. 111-2628-M-001-003-MY4, and the Academia Sinica (Project No. AS-CDA-109-M11). MRW also acknowledges supports from the Physics Division of the National Center for Theoretical Sciences, Taiwan. CYL acknowledges support from the National Center for High-performance Computing (NCHC). We acknowledge the following software: MATPLOTLIB [74], and NUMPY [75].

* z.xiong@gsi.de

† mwu@gate.sinica.edu.tw

‡ manug@gate.sinica.edu.tw

§ lincy@nchc.org.tw

- [1] H.-T. Janka, *Annu. Rev. Nucl. Part. Sci.* **62**, 407 (2012), [arXiv:1206.2503](#).
- [2] K.-C. Pan, C. Mattes, E. P. O’Connor, S. M. Couch, A. Perego, and A. Arcones, *J. Phys. G* **46**, 014001 (2019), [arXiv:1806.10030 \[astro-ph.HE\]](#).
- [3] A. Burrows, D. Vartanyan, J. C. Dolence, M. A. Skin-

- ner, and D. Radice, *Space Sci. Rev.* **214**, 33 (2018), [arXiv:1611.05859 \[astro-ph.SR\]](#).
- [4] S. Richers, H. Nagakura, C. D. Ott, J. Dolence, K. Sumiyoshi, and S. Yamada, *Astrophys. J.* **847**, 133 (2017), [arXiv:1706.06187 \[astro-ph.HE\]](#).
- [5] E. O’Connor, R. Bollig, A. Burrows, S. Couch, T. Fischer, H.-T. Janka, K. Kotake, E. J. Lentz, M. Liebendörfer, O. E. B. Messer, A. Mezzacappa, T. Takiwaki, and D. Vartanyan, *Journal of Physics G Nuclear Physics* **45**, 104001 (2018), [arXiv:1806.04175 \[astro-ph.HE\]](#).
- [6] A. Mezzacappa, E. Endeve, O. E. Bronson Messer, and S. W. Bruenn, *Liv. Rev. Comput. Astrophys.* **6**, 4 (2020), [arXiv:2010.09013 \[astro-ph.HE\]](#).
- [7] F. Foucart, *Liv. Rev. Comput. Astrophys.* **9**, 1 (2023), [arXiv:2209.02538 \[astro-ph.HE\]](#).
- [8] F. Capozzi and N. Saviano, *Universe* **8**, 94 (2022), [arXiv:2202.02494](#).
- [9] M. C. Volpe, arXiv e-prints (2023), [arXiv:2301.11814](#).
- [10] T. Fischer, G. Guo, K. Langanke, G. Martínez-Pinedo, Y.-Z. Qian, and M.-R. Wu, *Prog. Part. Nucl. Phys.* **137**, 104107 (2024), [arXiv:2308.03962 \[astro-ph.HE\]](#).
- [11] G. Sigl and G. Raffelt, *Nuclear Physics B* **406**, 423 (1993).
- [12] A. Vlasenko, G. M. Fuller, and V. Cirigliano, *Phys. Rev. D* **89**, 105004 (2014), [arXiv:1309.2628](#).
- [13] C. Volpe, *Int. J. Mod. Phys. E* **24**, 1541009 (2015), [arXiv:1506.06222](#).
- [14] A. Kartavtsev, G. Raffelt, and H. Vogel, *Phys. Rev. D* **91**, 125020 (2015), [arXiv:1504.03230 \[hep-ph\]](#).
- [15] D. N. Blaschke and V. Cirigliano, *Phys. Rev. D* **94**, 033009 (2016), [arXiv:1605.09383 \[hep-ph\]](#).
- [16] S. A. Richers, G. C. McLaughlin, J. P. Kneller, and A. Vlasenko, *Phys. Rev. D* **99**, 123014 (2019), [arXiv:1903.00022 \[astro-ph.HE\]](#).
- [17] R. F. Sawyer, *Phys. Rev. D* **79**, 105003 (2009), [arXiv:arXiv:0803.4319](#).
- [18] I. Izaguirre, G. Raffelt, and I. Tamborra, *Phys. Rev. Lett.* **118**, 021101 (2017), [arXiv:1610.01612 \[hep-ph\]](#).
- [19] F. Capozzi, B. Dasgupta, E. Lisi, A. Marrone, and A. Mirizzi, *Phys. Rev. D* **96**, 043016 (2017), [arXiv:1706.03360](#).
- [20] C. Yi, L. Ma, J. D. Martin, and H. Duan, *Phys. Rev. D* **99**, 063005 (2019), [arXiv:1901.01546 \[hep-ph\]](#).
- [21] T. Morinaga, *Phys. Rev. D* **105**, L101301 (2022), [arXiv:2103.15267](#).
- [22] B. Dasgupta, *Phys. Rev. Lett.* **128**, 081102 (2022), [arXiv:2110.00192](#).
- [23] M. R. Wu and I. Tamborra, *Phys. Rev. D* **95**, 103007 (2017).
- [24] M.-R. Wu, I. Tamborra, O. Just, and H.-T. Janka, *Phys. Rev. D* **96**, 123015 (2017), [arXiv:1711.00477 \[astro-ph.HE\]](#).
- [25] M. Delfan Azari, S. Yamada, T. Morinaga, W. Iwakami, H. Okawa, H. Nagakura, and K. Sumiyoshi, *Phys. Rev. D* **99**, 103011 (2019), [arXiv:1902.07467](#).
- [26] M. Delfan Azari, S. Yamada, T. Morinaga, H. Nagakura, S. Furusawa, A. Harada, H. Okawa, W. Iwakami, and K. Sumiyoshi, *Phys. Rev. D* **101**, 023018 (2020), [arXiv:1910.06176 \[astro-ph.HE\]](#).
- [27] H. Nagakura, T. Morinaga, C. Kato, and S. Yamada, *Astrophys. J.* **886**, 139 (2019), [arXiv:1910.04288](#).
- [28] T. Morinaga, H. Nagakura, C. Kato, and S. Yamada, *Phys. Rev. Res.* **2**, 012046(R) (2020), [arXiv:1909.13131](#)

- [astro-ph.HE].
- [29] S. Abbar, H. Duan, K. Sumiyoshi, T. Takiwaki, and M. C. Volpe, *Phys. Rev. D* **101**, 043016 (2020), arXiv:1911.01983.
- [30] M. George, M.-R. Wu, I. Tamborra, R. Ardevol-Pulpillo, and H.-T. Janka, *Phys. Rev. D* **102**, 103015 (2020), arXiv:2009.04046 [astro-ph.HE].
- [31] R. Glas, H.-T. Janka, F. Capozzi, M. Sen, B. Dasgupta, A. Mirizzi, and G. Sigl, *Phys. Rev. D* **101**, 063001 (2020), arXiv:1912.00274.
- [32] H. Nagakura, A. Burrows, L. Johns, and G. M. Fuller, *Phys. Rev. D* **104**, 083025 (2021), arXiv:2108.07281 [astro-ph.HE].
- [33] S. Abbar, F. Capozzi, R. Glas, H. T. Janka, and I. Tamborra, *Phys. Rev. D* **103**, 063033 (2021), arXiv:2012.06594.
- [34] A. Harada and H. Nagakura, *Astrophys. J.* **924**, 109 (2022), arXiv:2110.08291 [astro-ph.HE].
- [35] S. Richers, *Phys. Rev. D* **106**, 083005 (2022), arXiv:2206.08444.
- [36] J. D. Martin, C. Yi, and H. Duan, *Phys. Lett. B* **800**, 135088 (2020), arXiv:1909.05225 [hep-ph].
- [37] S. Bhattacharyya and B. Dasgupta, *Phys. Rev. Lett.* **126**, 061302 (2021), arXiv:2009.03337 [hep-ph].
- [38] S. Bhattacharyya and B. Dasgupta, *Phys. Rev. D* **102**, 063018 (2020), arXiv:2005.00459.
- [39] M.-R. Wu, M. George, C.-Y. Lin, and Z. Xiong, *Phys. Rev. D* **104**, 103003 (2021), arXiv:2108.09886 [hep-ph].
- [40] S. Richers, D. E. Willcox, N. M. Ford, and A. Myers, *Phys. Rev. D* **103**, 083013 (2021), arXiv:2101.02745.
- [41] S. Richers, D. Willcox, and N. Ford, *Phys. Rev. D* **104**, 103023 (2021), arXiv:2109.08631.
- [42] M. Zaizen and T. Morinaga, *Phys. Rev. D* **104**, 083035 (2021), arXiv:2104.10532 [hep-ph].
- [43] S. Abbar and F. Capozzi, *J. Cosmol. Astropart. Phys.* **2022**, 051 (2022), arXiv:2111.14880 [astro-ph.HE].
- [44] S. Richers, H. Duan, M.-R. Wu, S. Bhattacharyya, M. Zaizen, M. George, C.-Y. Lin, and Z. Xiong, *Phys. Rev. D* **106**, 043011 (2022), arXiv:2205.06282.
- [45] S. Bhattacharyya and B. Dasgupta, *Phys. Rev. D* **106**, 103039 (2022), arXiv:2205.05129.
- [46] E. Grohs, S. Richers, S. M. Couch, F. Foucart, J. P. Kneller, and G. C. McLaughlin, *Phys. Lett. B* **846**, 138210 (2023), arXiv:2207.02214.
- [47] M. Zaizen and H. Nagakura, *Phys. Rev. D* **107**, 103022 (2023), arXiv:2211.09343 [astro-ph.HE].
- [48] M. Zaizen and H. Nagakura, *Phys. Rev. D* **107**, 123021 (2023), arXiv:2304.05044 [astro-ph.HE].
- [49] Z. Xiong, M.-R. Wu, S. Abbar, S. Bhattacharyya, M. George, and C.-Y. Lin, *Phys. Rev. D* **108**, 063003 (2023).
- [50] H. Nagakura, L. Johns, and M. Zaizen, (2023), arXiv:2312.16285 [astro-ph.HE].
- [51] E. Grohs, S. Richers, S. M. Couch, F. Foucart, J. Froustey, J. P. Kneller, and G. C. McLaughlin, *Astrophys. J.* **963**, 11 (2024), arXiv:2309.00972 [astro-ph.HE].
- [52] J. Froustey, S. Richers, E. Grohs, S. D. Flynn, F. Foucart, J. P. Kneller, and G. C. McLaughlin, *Phys. Rev. D* **109**, 043046 (2024), arXiv:2311.11968 [astro-ph.HE].
- [53] Z. Xiong and Y.-Z. Qian, *Phys. Lett. B* **820**, 136550 (2021), arXiv:2104.05618 [astro-ph.HE].
- [54] S. Abbar, M.-R. Wu, and Z. Xiong, *Phys. Rev. D* **109**, 043024 (2024), arXiv:2311.15656.
- [55] S. Abbar, M.-R. Wu, and Z. Xiong, (2024), arXiv:2401.17424 [astro-ph.HE].
- [56] F. Capozzi, B. Dasgupta, A. Mirizzi, M. Sen, and G. Sigl, *Phys. Rev. Lett.* **122**, 091101 (2019), arXiv:1808.06618 [hep-ph].
- [57] H. Nagakura and M. Zaizen, *Phys. Rev. Lett.* **129**, 261101 (2022), arXiv:2206.04097 [astro-ph.HE].
- [58] Z. Xiong, M.-R. Wu, G. Martínez-Pinedo, T. Fischer, M. George, C.-Y. Lin, and L. Johns, *Phys. Rev. D* **107**, 083016 (2023), arXiv:2210.08254 [astro-ph.HE].
- [59] H. Nagakura and M. Zaizen, *Phys. Rev. D* **108**, 123003 (2023), arXiv:2308.14800 [astro-ph.HE].
- [60] H. Nagakura, *Phys. Rev. D* **108**, 103014 (2023), arXiv:2306.10108 [astro-ph.HE].
- [61] Z. Xiong, M.-R. Wu, M. George, C.-Y. Lin, N. K. Largani, T. Fischer, and G. Martínez-Pinedo, (2024), arXiv:2402.19252 [astro-ph.HE].
- [62] S. Shalgar and I. Tamborra, *Phys. Rev. D* **108**, 043006 (2023), arXiv:2206.00676 [astro-ph.HE].
- [63] S. Shalgar and I. Tamborra, *Phys. Rev. D* **107**, 063025 (2023), arXiv:2207.04058 [astro-ph.HE].
- [64] X. Li and D. M. Siegel, *Phys. Rev. Lett.* **126**, 251101 (2021), arXiv:2103.02616 [astro-ph.HE].
- [65] O. Just, S. Abbar, M. R. Wu, I. Tamborra, H. T. Janka, and F. Capozzi, *Phys. Rev. D* **105**, 083024 (2022), arXiv:2203.16559.
- [66] R. Fernández, S. Richers, N. Mulyk, and S. Fahlman, *Phys. Rev. D* **106**, 103003 (2022), arXiv:2207.10680 [astro-ph.HE].
- [67] J. Ehring, S. Abbar, H. T. Janka, G. Raffelt, and I. Tamborra, *Phys. Rev. D* **107**, 103034 (2023), arXiv:2301.11938.
- [68] J. Ehring, S. Abbar, H. T. Janka, G. Raffelt, and I. Tamborra, *Phys. Rev. Lett.* **131**, 061401 (2023), arXiv:2305.11207.
- [69] L. Johns, (2023), arXiv:2306.14982.
- [70] L. Johns, (2024), arXiv:2401.15247 [astro-ph.HE].
- [71] M. George, C.-Y. Lin, M.-R. Wu, T. G. Liu, and Z. Xiong, *Comput. Phys. Commun.* **283**, 108588 (2023), arXiv:2203.12866.
- [72] M. Zaizen and H. Nagakura, (2023), arXiv:2311.13842.
- [73] D. F. G. Fiorillo and G. Raffelt, (2024), arXiv:2403.12189 [hep-ph].
- [74] J. D. Hunter, *Computing in Science & Engineering* **9**, 90 (2007).
- [75] S. van der Walt, S. C. Colbert, and G. Varoquaux, *Computing in Science & Engineering* **13**, 22 (2011).